JACS
JOURNAL OF THE AMERICAN CHEMICAL SOCIETY

ARTICLE

pubs.acs.org/JACS

Solvent Evaporation Induced Aggregating Assembly Approach to Three-Dimensional Ordered Mesoporous Silica with Ultralarge Accessible Mesopores

Jing Wei,[†] Hai Wang,[†] Yonghui Deng,[*,†] Zhenkun Sun,[†] Lin Shi,[†] Bo Tu,[†] Mohammad Luqman,[‡] and Dongyuan Zhao[*,†]

[†]Department of Chemistry, Shanghai Key Laboratory of Molecular Catalysis and Innovative Materials, Advanced Materials Lab, Fudan University, Shanghai 200433, China

[‡]Chemical Engineering Department, College of Engineering, King Saud University, Kingdom of Saudi Arabia

Supporting Information

ABSTRACT: A solvent evaporation induced aggregating assembly (EIAA) method has been demonstrated for synthesis of highly ordered mesoporous silicas (OMS) in the acidic tetrahydrofuran (THF)/H_2O mixture by using poly(ethylene oxide)-*b*-poly(methyl methacrylate) (PEO-*b*-PMMA) as the template and tetraethylorthosilicate (TEOS) as the silica precursor. During the continuous evaporation of THF (a good solvent for PEO-*b*-PMMA) from the reaction solution, the template molecules, together with silicate oligomers, were driven to form composite micelles in the homogeneous solution and further assemble into large particles with ordered mesostructure. The obtained ordered mesoporous silicas possess a unique crystal-like morphology with a face centered cubic (fcc) mesostructure, large pore size up to 37.0 nm, large window size (8.7 nm), high BET surface area (508 m^2/g), and large pore volume (1.46 cm^3/g). Because of the large accessible mesopores, uniform gold nanoparticles (ca. 4.0 nm) can be introduced into mesopores of the OMS materials using the *in situ* reduction method. The obtained Au/OMS materials were successfully applied to fast catalytic reduction of 4-nitrophenol in the presence of $NaHB_4$ as the reductant. The supported catalysts can be reused for catalytic reactions without significant decrease in catalysis performance even after 10 cycles.

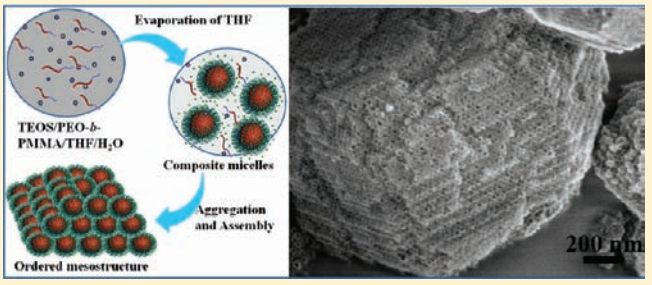

1. INTRODUCTION

Ordered mesoporous materials have received increasing attention in the past decades because of their potential applications in diverse fields, including adsorption,[1−3] separation,[4−7] catalysis,[8−13] drug delivery,[14−18] and fuel cells.[19−21] A great variety of mesoporous materials with controllable pore sizes and pore structures, tunable morphologies, and varying framework compositions have been synthesized via the soft-templating approach.[22−31] In general, the soft-templating syntheses are accomplished through the cooperative assembly of inorganic (or organic) precursors and amphiphilic surfactants (i.e., template molecules) based on electrostatic interaction, hydrogen binding, etc. To date, various soft templates, including small-molecular surfactants (cationic,[22] nonionic,[23] or anionic[24]) and high-molecular weight amphiphilic block copolymers,[32,33] have been exploited to synthesize ordered mesoporous materials.

Through the soft-templating approach, two main routes have been developed to synthesize ordered mesoporous materials, including solution-phase synthesis which usually requires a post hydrothermal treatment[23] and solvent evaporation induced self-assembly (EISA) method.[34−37] Small molecular surfactants (e.g., cetyltrimethylammonium bromide, CTAB) usually lead to ordered mesoporous materials (e.g., MCM-41) with pore size less than 5.0 nm which may limit their applications involving large objects. Ordered mesoporous materials with large pores have thus become a subject of extensive research, because the large mesopores can accommodate large-size guest objects in adsorption/immobilization of biomacromolecules and loading metal nanoparticles for catalysis without blocking the pore channels.[38−41] As is well-known, the pore size is mainly determined by the hydrophobic volume of the template molecules. Therefore, block copolymers with long hydrophobic chains enable ordered mesoporous materials with large pores. The most used high-molecular weight templates are commercial Pluronic type (i.e., poly(ethylene oxide)-*b*-poly(propylene oxide)-*b*-poly(ethylene oxide), PEO-PPO-PEO) triblock copolymers which have given rise to mesoporous materials with size less than 12 nm without using pore expanding agents.[11] Other block copolymers, such as poly(ethylene oxide)-*b*-polystyrene (PEO-*b*-PS),[33,42−45]

Received: August 16, 2011
Published: November 02, 2011

poly(isoprene)-*b*-poly(ethylene oxide) (PEO-*b*-PI),[32,46,47] poly(ethylene-*co*-butylene)-*b*-poly(ethylene oxide) (KLE),[48] and poly(ethylene oxide)-*b*-poly (methyl methacrylate) (PEO-*b*-PMMA)[49,50] have been also employed to synthesize mesoporous materials. Compared to PEO-PPO-PEO templates, these new synthetic templates have long rigid hydrophobic segments and high carbon contents. These features make them ideal templates for the synthesis of large-pore mesoporous materials and even those with crystallized frameworks, because they can be *in situ* carbonized in the pore channels and generate residual carbons that support the crystallization of the frameworks during high temperature treatment in inert atmosphere prior to combustion of carbon in air.[46,51] However, different from PEO-PPO-PEO block copolymers, because of their insolubility in water even in ethanol, all these templates have been limited to synthesize mesoporous materials through the EISA approach. Synthesis of ordered mesoporous materials, including silica, carbon, and metal oxide, in aqueous solutions by using these templates is still a big challenge. Previously, a self-organized precipitation (SORP) method has been demonstrated to synthesize the block copolymer particles with well-defined phase separation structure, which features the evaporation of good solvent leads to the formation and organization of block copolymer particles in the remaining bad solvent.[52−55] These results suggest a possibility to synthesize mesoporous materials in solution phase by using the above-mentioned synthetic templates. Solution-phase syntheses have proved beneficial for mass production of mesoporous materials with diverse morphologies (spheres, polyhedrons, fibers, helical rods) which are highly desirable in practical applications. To date, little work has been reported to synthesize ordered mesoporous materials with accessible pores by using these templates with strong hydrophobic segments in aqueous-phase system. Consequently, development of new solution-phase synthesis strategies for large-pore mesoporous materials using the block copolymers with long hydrophobic segments is of great importance.

Herein, we report a solvent evaporation induced aggregating assembly (EIAA) method to synthesize highly ordered mesoporous silica (OMS) materials by using homemade water insoluble block copolymer PEO-*b*-PMMA as a template, tetraethylorthosilicate (TEOS) as a precursor, and acidic tetrahydrofuran (THF)/H_2O mixture as the reaction medium. Different from the commonly used EISA method where only a calculated amount of water is permitted to be used in the initial solution, and the ordered mesostructure is formed at the interface of the solid (substrate)−liquid (solution) when the solvent evaporates off, our method is more tolerant to water, and the self-assembly occurs at the liquid−liquid interface. The as-made products were found to consist of unique particles with large dimension of 0.5−6 μm and distinct crystal-like morphology. After the hydrothermal treatment and calcination, the obtained mesoporous silica materials have a face centered cubic (fcc) mesostructure ($Fm\bar{3}m$), large tunable pore size of ∼37.0 nm, large window size (∼8.7 nm), high surface area, and large pore volume. By virtue of the highly accessible large mesopore size, small gold nanoparticles could be introduced into the mesopores of the OMS materials and retained stably on the surface of the large pore cages. The obtained Au/OMS materials were successfully applied to fast catalytic reduction of 4-nitrophenol in the presence of $NaHB_4$ as a reductant, and they can be reused without significant decrease in catalytic performance even after 10 cycles.

2. EXPERIMENTAL SECTION

2.1. Chemicals. Monomethoxy poly(ethylene oxide) (PEO_{5k} and PEO_{2k} with M_w of 5000 and 2000 g/mol, respectively) and 2-bromoisobutyryl bromide were purchased from Aldrich. *N*,*N*,*N*′,*N*′,*N*″-Pentamethyldiethylenetriamine (PMDETA) was purchased from Acros. Methyl methacrylate (MMA), tetrahydrofuran (THF) (>99%), pyridine (>99%), cuprous chloride (CuCl), tetraethylorthosilicate (TEOS) (AR), hydrochloric acid, 4-nitrophenol (4-NP), sodium borohydride ($NaBH_4$), $HAuCl_4 \cdot 4H_2O$, and anhydrous ethylether (>99%) were purchased from Shanghai Chemical Corp. MMA was purified by filtration using an Al_2O_3 column to remove the polymerization inhibitor. Millipore water was used in all experiments.

2.2. Synthesis of the Block Copolymers. The block copolymers EO_{125}-*b*-MMA_{174} (PDI: 1.09) and EO_{44}-*b*-MMA_{103} (PDI: 1.07) were synthesized by using an atom transfer radical polymerization (ATRP) technique which involves two steps, i.e., preparation of the macroinitiator, and polymerization of MMA monomers.[50] Typically, 20.0 g of monomethoxy poly(ethylene oxide) PEO_{5k} (M_w: 5000 g/mol) was dissolved in a solvent mixture of THF (60 mL) and pyridine (40 mL). The resulting solution was cooled in an ice−water bath followed by adding 3.00 g of 2-bromoisobutyryl bromide with stirring. Afterward, the solution was stirred at 30 °C for 12 h and then filtrated to obtain a homogeneous solution. Subsequently, 200 mL of cold ether was added to the solution to obtain white precipitates which were collected by filtration and then washed with ether. After being dried in vacuum at 25 °C, PEO_{5k}-Br macroinitiator was obtained. In the next step, EO_{125}-*b*-MMA_{174} was prepared by polymerizing MMA using PEO_{5k}-Br as an initiator. 2.5 g of PEO_{5k}-Br, 0.50 g of CuCl, 10 mL of MMA, 0.22 g of PMDETA, and 20 mL of THF were added into an ampule bottle. After removal of air by bubbling with Ar gas for 30 min, the reaction system was sealed and placed in a thermostatted oil bath at 60 °C for polymerization under stirring. After 5 h, the system was cooled to room temperature, and 50 mL of THF was added to dissolve the product. The obtained solution was filtrated through an Al_2O_3 column to remove the Cu complex. Cold ether (200 mL) was poured into the filtrate to precipitate diblock copolymer PEO-*b*-PMMA. The product was collected by filtration and dried under vacuum. Similarly, EO_{44}-*b*-MMA_{103} was prepared using PEO_{2k}-Br as macroinitiator through the same procedure by using 1.5 g of PEO_{2k}-Br, 0.078 g of CuCl, 10 mL of MMA, 0.14 g of PMDETA, and 20 mL of THF. The reaction time was 4 h.

2.3. Synthesis of Ordered Mesoporous Silica. The ordered mesoporous silica samples were synthesized via the solvent evaporation induced aggregating assembly (EIAA) method in an acidic mixed solvent of THF and water by using TEOS as a silica source and diblock copolymer PEO-*b*-PMMA with different molecular weight as a template. For a typical preparation, 7.0 g of THF solution of EO_{125}-*b*-MMA_{174} (0.57 wt %) was mixed with 2.0 g of HCl solution (2 M) with stirring. Then, 0.30 g of TEOS was added into the above transparent solution. The composition of EO_{125}-*b*-MMA_{174}/THF/2 M HCl/TEOS mass ratio is 1:175:50:7.5. After that, the solution was left to stand for evaporation of THF at 25 °C in air in a hood. After 48 h, white silica/PEO-*b*-PMMA composites were precipitated from the solution and collected by centrifugation, washed with water three times, and dried at 25 °C. The as-made silica-EO_{125}-MMA_{174} sample was hydrothermally treated at 100 and 130 °C for 24 h, respectively, and then calcined at 550 °C in air for 5 h to remove the template. Through the same approach, EO_{44}-*b*-MMA_{103} block copolymer was also used as a template to synthesize mesoporous silica, and the optimized composition for EO_{44}-*b*-MMA_{103}/THF/2 M HCl/TEOS mass ratio is 1:100:50:10.

2.4. Loading Au Nanoparticles onto the Ordered Mesoporous Silica. Gold nanoparticles were loaded onto the mesoporous silica according to previous report.[56] Typically, 50 mg of ethylenediamine (en) was added to 1.0 mL of aqueous solution of $HAuCl_4 \cdot 4H_2O$ (0.10 g in 1.0 g of H_2O) under stirring until a transparent brown solution was formed.

Upon addition of ethanol (8 mL), the precipitate of $AuCl_3(en)_3$ was immediately formed, collected by filtration, washed with water, and dried under vacuum oven at 40 °C. $AuCl_3(en)_3$ (10 mg) was dissolved in 5 mL of H_2O, and the pH value was adjusted to 10.0 by using a NaOH solution (5.0 wt %). Subsequently, 60 mg of the calcined mesoporous silica samples templated from EO_{125}-*b*-MMA_{174} after the hydrothermal treatment at 100 °C was dispersed in the aqueous solution of $AuCl_3(en)_3$ with stirring. After 1 h, the sample was separated by centrifugation, quickly washed with water, and dried in vacuum oven at 40 °C for 2 days. The sample was then subjected to reduction by flowing H_2/Ar (5.0%) at 150 °C for 1 h, resulting in Au/OMS composites.

2.5. Catalytic Reduction of 4-Nitrophenol (4-NP). The reduction of 4-NP was carried out in a quartz cuvette and monitored by using a UV−vis spectroscopy (Jasco V-550) at 25 °C. A 35 mg portion of of 4-NP solution (0.0757 g of 4-NP dissolved in 100 mL of H_2O) was added to 1.00 g of $NaBH_4$ solution (0.02 g in 3.0 mL of H_2O). Subsequently, 100 mg of aqueous dispersion of the Au/OMS composite (0.02 wt %) was added, and the solution was quickly subjected to UV−vis measurements for monitoring the absorption changes during the reaction.

2.6. Measurement and Characterization. Small angle X-ray scattering (SAXS) measurements were taken on a Nanostar U small-angle X-ray scattering system (Bruker, Germany) using Cu Kα radiation (40 kV, 35 mA). The *d*-spacing values were calculated from the formula $d = 2\pi/q$. Nitrogen sorption isotherms were measured at 77 K with a Micromeritics Tristar 3020 analyzer (USA). Before measurements, the samples were degassed in a vacuum at 180 °C for at least 6 h. The Brunauer−Emmett−Teller (BET) method was utilized to calculate the specific surface areas. By using the Broekoff−de Boer (BdB) sphere model, the pore volumes and pore size distributions were derived from the adsorption branches of isotherms, and the total pore volumes (V) were estimated from the adsorbed amount at a relative pressure P/P_0 of 0.995. The window size was calculated from the desorption branches. Transmission electron microscopy (TEM) experiments were conducted on a JEOL 2011 microscope (Japan) operated at 200 kV. Field-emission scanning electron microscopy (FESEM) images were collected on the Hitachi model S-4800 field emission scanning electron microscope. The dried samples were directly used for the observation without any treatment. To obtain information during the EIAA process, cryo-scanning electron microscopy (Cryo-SEM) images were taken on the samples functioned with the evaporation time. A small amount of reactant solution (0.5 mL) was withdrawn at different stages during the solvent evaporation. The solution was dropped on a concave copper sample holder and quickly emerged into a soil nitrogen (a kind of semisolid nitrogen made by treating liquid nitrogen under vacuum) to form a solid specimen. The solid sample was microtomed for the cryo-SEM observations. The UV−vis spectra were recorded on a UV−vis spectrometer (Jasco V-550) at 25 °C. X-ray diffraction (XRD) patterns were recorded with a Bruker D8 powder X-ray diffractometer using Cu Kα radiation (40 kV, 40 mA). The dynamic light scattering (DLS) spectra were measured at 25 °C on Zetasizer instrument (ZS-90, Malvern).

3. RESULTS AND DISCUSSION

PEO-*b*-PMMA copolymers with long PMMA chains were synthesized via the atom transfer radical polymerization (ATRP) method. The template molecules obtained after 5 h polymerization were measured and calculated to have a weight average molecular weight (M_w) of around 22 500 g/mol with polydispersity index (PDI) of 1.09. Correspondingly, the composition can be approximately formulated as EO_{125}-*b*-MMA_{174}. Due to the hydrophobic property of PMMA, the block copolymers are insoluble in water. To overcome this insolubility problem and carry out the synthesis of ordered mesoporous silica materials in aqueous solution, PEO-*b*-PMMA templates were first dissolved

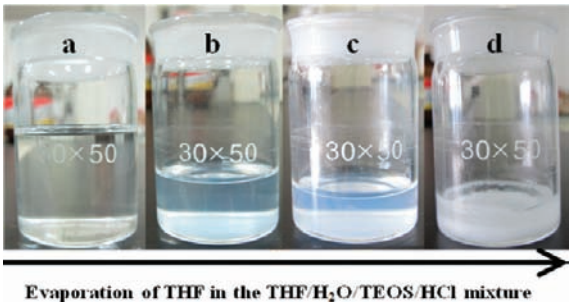

Figure 1. Photographs of the solution after evaporation of THF for (a) 0, (b) 10, (c) 30, and (d) 48 h.

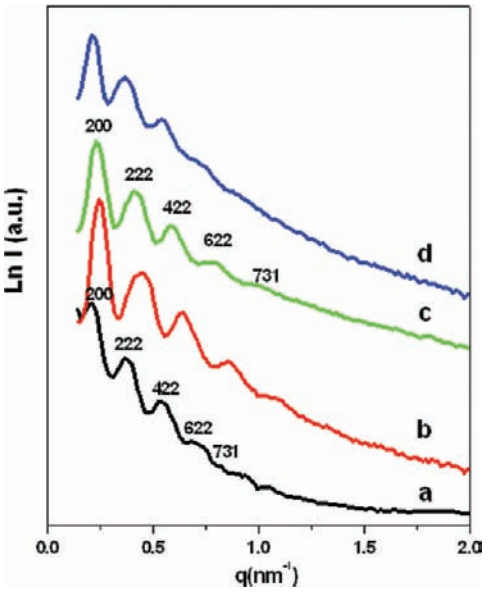

Figure 2. SAXS patterns of (a) the as-made mesoporous silica, i.e., silica-EO_{125}-MMA_{174}, (b) silica-EO_{125}-MMA_{174}-550 obtained after direct calcination at 550 °C in air, (c) silica-EO_{125}-MMA_{174}-100-550 obtained after hydrothermal treatment at 100 °C and then calcination at 550 °C in air, and (d) silica-EO_{125}-MMA_{174}-130-550 obtained after hydrothermal treatment at 130 °C and then calcination at 550 °C in air.

in a large amount of THF which is a good solvent for both PMMA and PEO.

Hydrochloric acid aqueous solution and TEOS were then added sequentially to obtain a homogeneous solution (Figure 1a, 0 h). In this way, other synthetic templates, such as PEO-*b*-PS, can also be dissolved for templating synthesis of mesoporous materials in aqueous solution. As THF evaporates slowly under static conditions at room temperature, the reaction solution experienced dramatic changes from a clear solution, to a slightly blue colloidal solution (Figure 1b, 10 h), to a milky white dispersion (Figure 1c, 30 h), and finally to a suspension with white precipitates (Figure 1d, 48 h). SAXS patterns of the as-made silica-template composite (denoted as-made silica-EO_{125}-MMA_{174}) obtained by using EO_{125}-*b*-MMA_{174} as the templates (Figure 2a) show five scattering peaks with q-values of 0.213, 0.370, 0.526, 0.710, 0.826 nm^{-1}, which can be indexed to the 200, 222, 422, 622, and 731 reflections of highly ordered fcc mesostructure with space group of $Fm\bar{3}m$. The unit cell parameter (a_0) calculated from the SAXS data is about 59.0 nm, indicative of an ultralarge

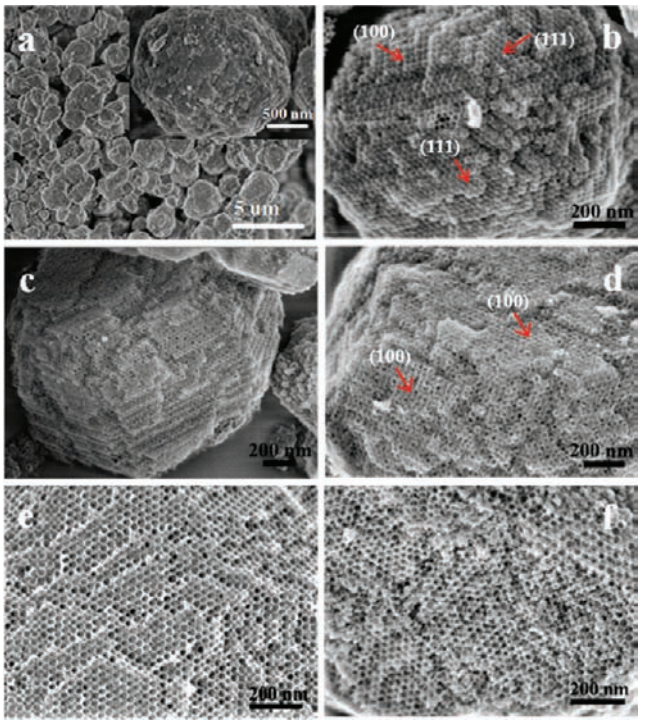

Figure 3. FESEM images of (a, b) as-made silica-EO_{125}-MMA_{174}, (c, d) silica-EO_{125}-MMA_{174}-550 obtained after direct calcination at 550 °C in air, (e) silica-EO_{125}-MMA_{174}-100-550 obtained after the hydrothermal treatment at 100 °C and then calcination at 550 °C in air, and (f) silica-EO_{125}-MMA_{174}-130-550 obtained after hydrothermal treatment at 130 °C and then calcination at 550 °C in air.

unit. After direct calcination at 550 °C in air to remove the templates, SAXS patterns of the obtained mesoporous silica (denoted as silica-EO_{125}-MMA_{174}-550) show more resolved five scattering peaks with higher diffraction intensity (Figure 2b), suggesting that the ordered mesostructure is stable and well retained. Compared with the as-made sample, the calcined mesoporous silica has a smaller cell parameter of 51.9 nm, reflecting significant structure shrinkage of 12% due to the further framework cross-linking. The mesoporous silica (denoted silica-EO_{125}-MMA_{174}-100-550) obtained after being hydrothermally treated at 100 °C and then calcined at 550 °C (Figure 2c) exhibits similar SAXS patterns with peaks shifted to lower q values, indicating a thermally stable mesostructure. Compared to that (51.9 nm) of the sample after direct calcination at 550 °C, the larger unit cell parameter (55.1 nm) is observed, suggesting a pronounced structural expansion (6.2%) exerted by the hydrothermal treatment. The mesoporous silica sample (denoted silica-EO_{125}-MMA_{174}-130-550) after a higher temperature hydrothermal treatment (130 °C) shows a slightly poor SAXS pattern with three scattering peaks (Figure 2d), suggesting that the mesostructure is partially degenerated, which is caused by the intense expansion of templates. The unit cell parameter is calculated to be as large as ~59.0 nm, corresponding to a further structural expansion of about 7.5%.

FESEM images show that the as-made mesoporous silica templated by diblock copolymer EO_{125}-*b*-MMA_{174} consists of particles with the size ranging from 0.5 to 6 μm (Figure 3a). Interestingly, most of the particles possess crystal-like morphology with distinct planes and edges (Figure 3b). Uniform nanospheres in each plane are found to arrange with remarkably high

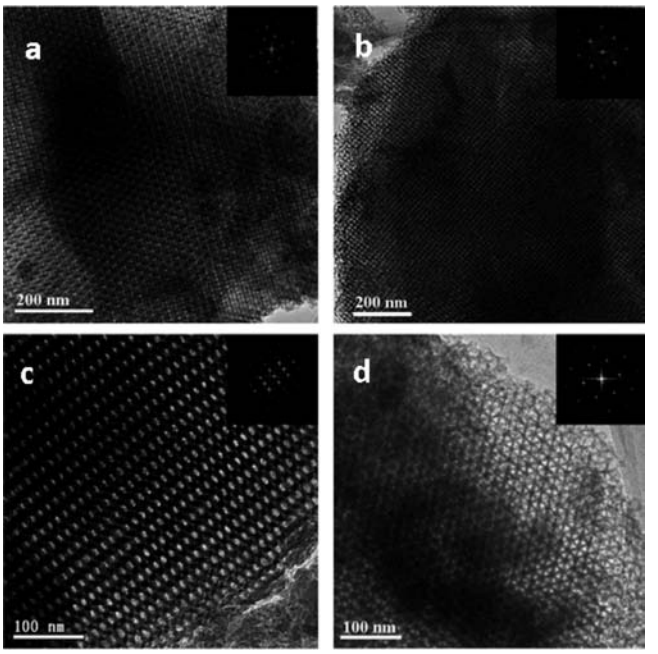

Figure 4. TEM images of the mesoporous silica-EO_{125}-MMA_{174}-100-550 sample obtained after hydrothermal treatment at 100 °C and then calcination at 550 °C in air: (a) 110, (b) 100, (c) 211, and (d) 111 directions. The insets are the corresponding FFT images.

regularity with typical planes of a colloidal crystal with an fcc structure as marked in the FESEM image (Figure 3b). It implies a spherical packing process of the particles with an ordered mesostructure during the good-solvent evaporation induced aggregating assembly process, which is similar to the atomic crystal growth. After direct calcination at 550 °C, the obtained mesoporous silica particles retain crystal-like morphologies, suggesting a stable framework (Figure 3c). Due to the removal of templates, highly ordered arrays of hollow nanospheres with small openings could be clearly visible on the particle surface (Figure 3d). Compared to the as-made sample, the mesoporous silica obtained after the hydrothermal treatment at 100 °C shows much larger opening mesopores (Figure 3e). Hydrothermal treatment at higher temperature (130 °C) results in more opened mesopores (Figure 3f), owing to the intense swelling of templates. It is worth noting that the samples prepared without the addition of TEOS have mixed morphology of nanospheres and nanorods due to the assembly of the template molecules (Figure S1). It suggests that the silica source plays a key role in the formation of the ordered mesostructure during the self-assembly process. TEM images and corresponding fast Fourier transforms (Figure 4a–d) show that the calcined mesoporous silica sample after being hydrothermally treated at 100 °C (silica-EO_{125}-MMA_{174}-100-550) has a high degree of periodicity viewed from [110], [100], [211], and [111] directions, respectively. It further confirms the silica mesostructure templated from the copolymer EO_{125}-*b*-MMA_{174} through the unique EIAA approach has a highly ordered cubic symmetry ($Fm\bar{3}m$). The uniform and large spherical pores can be clearly observed in the images. It implies that the ordered mesoporous silicas are constructed through the close packing of uniform spherical micelles. The unit cell parameter of the calcined mesoporous silica sample after hydrothermal treatment at 100 °C is estimated from the TEM image to be ~53.8 nm, in good agreement with that (55.1 nm) from SAXS data.

dx.doi.org/10.1021/ja207525e |*J. Am. Chem. Soc.* 2011, 133, 20369–20377

N_2 sorption isotherms of the mesoporous silica templated by diblock copolymer EO_{125}-*b*-MMA_{174} after being directly calcined at 550 °C (denoted silica-EO_{125}-MMA_{174}-550) exhibit representative type IV curves with a sharp capillary condensation step in the relative pressure range 0.85−0.94 (Figure 5A, a). It indicates that ultralarge uniform mesopores are generated. A large H_2-type hysteresis loop with delayed capillary evaporation located at a P/P_0 of about 0.50 is observed, revealing caged mesopores with a window size smaller than 5.0 nm.[57] Comparatively, the mesoporous silica samples obtained with hydrothermal treatment at 100 and 130 °C (Figure 5b, c) show representative type IV isotherms with sharp capillary condensation steps at higher relative pressure ranges of 0.86−0.96 and 0.88−0.98, respectively, indicative of larger mesopores with very uniform size. It should be noted that the hysteresis loops become smaller and desorption branches shift to higher relative pressure as the hydrothermal temperature increases from 100 to 130 °C. The sample silica-EO_{125}-MMA_{174}-130-550 even shows an H_1 type hysteresis loops, indicating a continuous increase of the entrance sizes of mesopores. The pore size distributions derived from the adsorption branches based on the Broekoff−de Boer (BdB) sphere model[58] show that all the samples have uniform mesopores. The pore sizes increase dramatically from 32.9 to 37.0 and 44.6 nm with the increase of the hydrothermal temperature (Figure 5B). Calculations from the desorption branches reveal that the entrance sizes increase from about 4.0 to 8.7, and 11.8 nm, respectively, corresponding to a significant increase of window size up to 300% (Table 1).

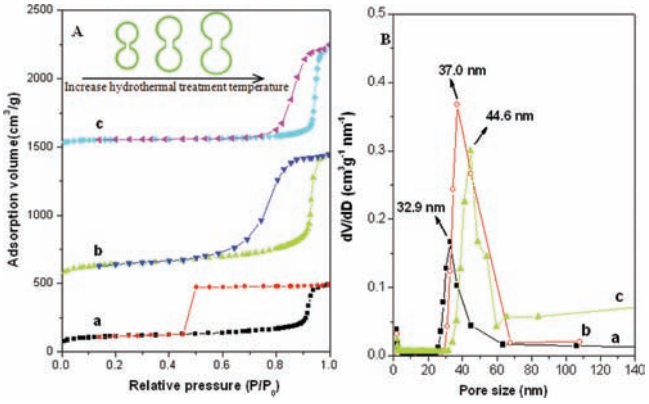

Figure 5. N_2 sorption isotherms (A) and pore size distributions (B) of the ordered mesoporous silica prepared using EO_{125}-*b*-MMA_{174} as a template, (a) silica-EO_{125}-MMA_{174}-550 obtained by direct calcination at 550 °C in air, (b) silica-EO_{125}-MMA_{174}-100−550 after hydrothermal treatment at 100 °C and then calcination at 550 °C in air, and (c) silica-EO_{125}-MMA_{174}-130−550 obtained after hydrothermal treatment at 130 °C and then calcination at 550 °C in air. For clarity, the isotherm curves were offset by (b) 500 and (c) 1500 cm^3/g, respectively. The inset in panel A schematically illustrates the pore expanding process during hydrothermal treatment.

The mesoporous silica obtained after direct calcination possesses a surface area of 400 cm^2/g, pore volume of 0.76 cm^3/g, and micropore surface area of 191 m^2/g. While silica-EO_{125}-MMA_{174}-100-550 has a higher surface area (508 m^2/g), larger pore volume (1.46 cm^3/g), and lower micropore surface area (130 m^2/g). The increase of surface area and pore volume could be due to the fact that the hydrothermal treatment can make mesopores opened and thus facilitate the combustion of templates during calcination in air. The silica-EO_{125}-MMA_{174}-130-550 sample possesses a relatively lower surface area (193 m^2/g) and smaller pore volume (1.16 m^3/g), which is due to the partially collapsed porous structure.

Block copolymers (EO_{44}-*b*-MMA_{103}) with the same composition but lower molecular weight (M_w = 12500 g/mol, PDI = 1.07) can also be used as a template to synthesize ordered mesoporous silicas by the novel EIAA approach. Similarly, the obtained mesoporous silica (denoted silica-EO_{44}-MMA_{103}-550) after direct calcination at 550 °C in air shows well-resolved SAXS patterns for a highly ordered fcc ($Fm\bar{3}m$) mesostructure (Figure S2). Calculation from the SAXS patterns indicates that, after the hydrothermal treatment at 100 °C, the unit cell parameter can increase from 32 to 40 nm. These values are much smaller than those of the corresponding samples templated from EO_{125}-*b*-MMA_{174} with longer PMMA chains, because the latter can assemble into larger micelles. TEM images of the mesoporous silica templated from the small copolymer EO_{44}-*b*-MMA_{103} after the hydrothermal treatment at 100 °C (Figure S3) show highly

Table 1. Textual Properties of the Ordered Mesoporous Silica Samples Prepared via the Solvent Evaporation Induced Aggregating Assembly Approach by Using PEO-*b*-PMMA as a Template, TEOS as the Silica Source, and Acidic THF/H_2O (8/2, V/V) Mixture as the Solvent

sample	unit cell parameter (a_0) (nm)	pore size (nm)	window size[d] (nm)	BET surface area[e] (m^2/g)	pore volume (cm^3/g)	micropore surface area[f] (m^2/g)
as-made silica-EO_{125}-MMA_{174}[a]	59.0					
silica-EO_{125}-MMA_{174}-550[b]	51.9	32.9	<5	400	0.76	191
silica-EO_{125}-MMA_{174}-100-550[c]	55.1	37.0	8.7	508	1.46	130
silica-EO_{125}-MMA_{174}-130-550	59.0	44.6	11.8	193	1.16	96
silica-EO_{44}-MMA_{103}-550	29.4	18.0	<5	330	0.72	127
silica-EO_{44}-MMA_{103}-100-550	35.3	24.4	<5	499	1.11	47

[a] The as-made silica-template composite sample obtained via the EIAA method by using EO_{125}-*b*-MMA_{174} as a template. [b] The mesoporous silica sample obtained after direct calcination of the as-made sample at 550 °C in air. [c] The mesoporous silica sample obtained after the hydrothermal treatment at 100 °C and then calcination at 550 °C in air. [d] Calculated by BdB model from the adsorption branches of N_2 sorption isotherms. [e] Calculated from the desorption branches. [f] Calculated by the V−*t* method.

dx.doi.org/10.1021/ja207525e |*J. Am. Chem. Soc.* 2011, 133, 20369–20377

ordered cubic mesostructure ($Fm\bar{3}m$ symmetry) viewed from [100], [110], and [211] directions, respectively. Large spherical pores of about 24 nm can be clearly observed, further confirming a close packing of spherical micelles during the EIAA process. N_2 sorption isotherms of all the mesoporous silicas templated from the small copolymer EO_{44}-*b*-MMA_{103} show type IV curves with a large hysteresis loop, suggesting a uniform cagelike mesopore. The pore size is significantly increased from 18.0 to 24.4 nm after the hydrothermal treatment (Figure S4). The surface area and pore volume are in the range 330−499 m^2/g and 0.72−1.11 cm^3/g, respectively (Table 1), which are a little smaller than that templated from EO_{125}-*b*-MMA_{174} with longer PMMA chains.

To acquire more detailed information during the solvent evaporation induced aggregating assembly, cryo-SEM combined with TEM technique was employed to characterize the solutions withdrawn from the reaction vial at different times. Before the electron microscopy analysis, the samples were frozen by soil nitrogen and microtomed. In the beginning, the reaction solution (∼10 mL in volume, [HCl] = 0.4 M, THF/H_2O v/v = 8:2) is clear and transparent. After standing for 10 h, a considerable amount of THF (∼4 mL) was evaporated off (in this case the volume ratio of THF/H_2O is about 2:1 in the solution). The solution turned into a homogeneous light-blue colloidal system. The cryo-SEM image shows that uniform nanospheres are formed and well dispersed in the remained solution (Figure S5a). The TEM image clearly shows that the nanospheres possess a typical core−shell structure with PEO-*b*-PMMA as a core and silica as a shell (Figure S6a). After calcination at 550 °C in air, uniform hollow silica nanospheres can be obtained at this step (Figure S6b). It confirms that every nanosphere represents a composite micelle with a block copolymer core and silica shell. Moreover, this result suggests that we can prepare uniform and large pore mesoporous silica hollow spheres by simply stopping the reaction in this step. The solution was further concentrated after standing for 36 h with about 6.5 mL of THF evaporated (the volume ratio of THF/H_2O is about 0.75:1 in the solution), and tiny aggregates were observed in the remaining milky white solution, implying that the composite micelles start to assemble at the high concentration of micelles and acidity on the interface of poor-solvent water phase. It is evidenced by the cryo-SEM image where the nanospheres tend to approach and aggregate each other (Figure S5b). After further evaporation for about 0.5 h, large aggregates can be found to gradually precipitate from the solution, indicating an accelerated assembly of micelles. The cryo-SEM images indicate that these aggregates are large particles made of closely packed nanospheres (Figure S5c). After standing for 48 h, with most of the THF evaporated off (the volume ratio of THF/H_2O reaches 0.5:1, [HCl] = 1.5 M), large precipitates were observed in the remained solution. The cross-section image of the granular aggregates (Figure S5d, and insert) shows a highly ordered mesostructure of closely packed nanospheres. It suggests that the composite micelles assemble into ordered mesostructure via sphere packing, which is evidenced by the FESEM image of the entire particles (Figure 3b).

Additionally, dynamic light scattering (DLS) was used to monitor the evolution of particles formed during the EIAA process. The results show that the original solution contains ultrasmall PEO-*b*-PMMA unimers with hydrodynamic diameter of about 3.6 nm (Figure S7a). After 14 h, two new peaks at 0.62 and 47.5 nm were observed, which are attributed to the silica oligomers and PEO-*b*-PMMA micelles, respectively (Figure S7b).

Scheme 1. Formation Mechanism of Ordered Mesoporous Silica through the Solvent Evaporation Induced Aggregating Assembly (EIAA) Process by Using Diblock Copolymer PEO-*b*-PMMA as a Template, TEOS as the Silica Source, and Acidic THF/H_2O Mixture as the Solvent[a]

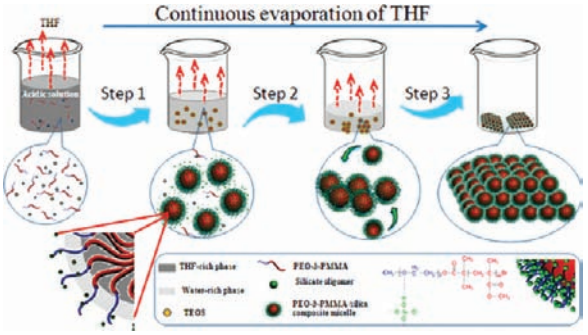

[a] Step 1: the formation of the hybrid PEO-*b*-PMMA/SiO_2 spherical micelles with PMMA as a core and silica-associated PEO as a shell with the evaporation of THF. Step 2: the packing of the uniform hybrid micelles into closed-packing fcc mesostructure on the interface of the poor solvent water-rich phase, which is driven by the ever-increasing concentration of the composite micelles and the requirement of minimization of interface energy. Step 3: the accelerated cross-linking and condensation of the silicate oligomers for fixing the ordered mesostructure, which is caused by the increased acidity of the reaction solution due to further evaporation of THF.

The peak at 3.6 nm reveals that at this stage the concentration is not high enough, and a considerable amount of PEO-*b*-PMMA still remains as unimers. After 17 h, the size of the silica oligomer increases to 1.5 nm due to the further hydrolysis and condensation of the silica source. The disappearance of the peak at 3.6 nm suggests that most of the PEO-*b*-PMMA polymers assemble with silicate oligomers into composite micelles with the size of about 35 nm (Figure S7c). After 20 h, the peak at around 4.8 nm assigned to pure silicate nanoparticles is detected; meanwhile larger particles attributed to the aggregation of the PEO-*b*-PMMA/silicate composite micelles began to appear at hundreds of nanometers and even several micrometers (Figure S7d,e). It suggests that the composite micelles gradually assemble into ordered mesostructured large particles. The DLS results for the sample obtained after evaporation for longer time are not accurate because the particles begin to precipitate from the solution.

To the best of our knowledge, this is the first report on the synthesis of highly ordered mesoporous materials by using high-molecular-weight water-insoluble block copolymer as a template in aqueous solution phase. On the basis of the aforementioned results, we believe that the successful synthesis of ordered mesoporous silica with ultralarge pore is indebted to the unique assembly process of the good-solvent evaporation induced aggregation (Scheme 1). The water-insoluble block copolymer PEO-*b*-PMMA can be dissolved in a THF/H_2O solution with a high volume ratio (v/v 8:2), because THF is a good solvent for the copolymer templates. As THF evaporates, the solvency power of the mixed solvent decreases significantly because water is a poor solvent for the hydrophobic PMMA, and thus PMMA segments tend to aggregate. On the other hand, water is a good solvent for PEO segments. These two factors drive the PEO-*b*-PMMA molecules to form spherical micelles with PMMA as a core surrounded by PEO shell on the interface of the water-rich

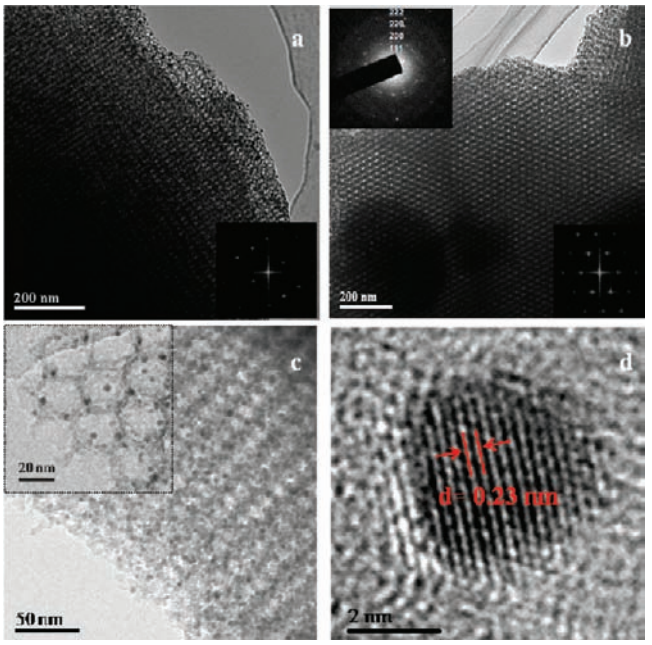

Figure 6. TEM images of Au/OMS viewed from 211 (a, c) and 110 (b) directions. Insert in part c is the enlarged TEM image viewed from 111 directions. (d) High resolution TEM image of Au nanoparticles.

phase. Simultaneously, silicate oligomers hydrolyzed from TEOS catalyzed by the acid in water-rich solution can associate with PEO moieties through hydrogen bonding, giving rise to a blue colloidal dispersion of tiny silicates/PEO-*b*-PMMA composite micelles on the interface between the THF-rich and water-rich phases (Scheme 1, step 1). With the continuous loss of the good solvent THF, the spherical composite micelles are continually formed. The ever-increasing concentration of the tiny colloids drives the spherical composite micelles to attach with each other and slowly aggregate into particles to decrease interface energy (Scheme 1, step 2). During this period, the spherical composite micelles as building blocks adopt a preferable fcc packing because it is stable from the viewpoint of thermodynamics.[59] The increasing acidity of the solution accelerates the cross-linking and condensation of silicate oligomers from the water-rich phase, thus fixing the ordered PEO-*b*-PMMA/SiO_2 mesostructure in a short time. As a result, large crystal-like particles are formed, precipitated, and separated from the solution phase (Scheme 1, step 3). Therefore, the solvent evaporation induced aggregating assembly can be viewed as a packing process of the composite micelles as building blocks in a "layer-by-layer" manner, similar to the growth of an atomic crystal. During the subsequent hydrothermal treatment at 100 °C, the PEO segments can be withdrawn from the silica pore walls and the PEO-*b*-PMMA templates are significantly swollen; meanwhile, the silicate frameworks undergo an intense reorganization due to the further cross-linking and condensation. These two opposite effects may lead to the cracking of the silica walls and the formation of the large mesopore windows, which also favors the combustion of PEO-*b*-PMMA templates during calcination in air. Therefore, compared to the sample after the direct calcination, the mesoporous silica obtained after the hydrothermal treatment has larger pore and window sizes, and higher surface area. However, too high treatment temperature (130 °C) can partially destroy the pore structure, resulting in a poor mesostructure and low surface areas.

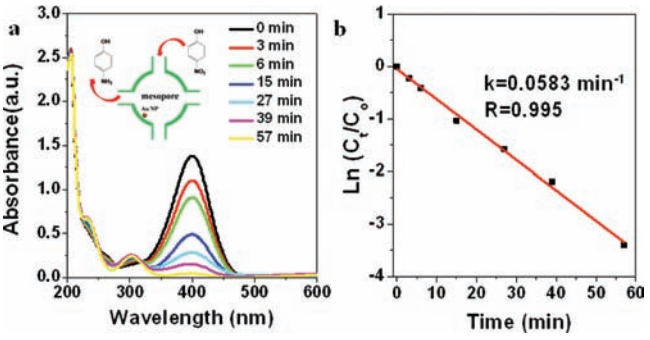

Figure 7. (a) UV−vis absorption spectra recorded during the catalytic reduction of 4-NP over the Au/OMS composite at 25 °C, indicating a continuous decrease of absorbance of 4-nitrophenol (4-NP) at around 400 nm. The insert in panel a schematically illustrates the catalytic reduction. (b) The relationship between $\ln(C_t/C_0)$ and reaction time (t), wherein the ratios of 4-NP concentration (C_t at time t) to its initial value C_0 (t = 0) were directly given by the relative intensity of the respective absorbance A_t/A_0, and therefore, the reduction course could be directly reflected by these absorption curves.

The ordered mesoporous silica particles obtained through the unique EIAA approach is particularly suitable for loading functional nanoparticles for catalysis because of the high accessibility of their 3-D mesostructure with large pore cages and windows. In this study, Au nanoparticles were introduced into the large spherical mesopores via the wet-impregnation and hydrogen reduction.[56] The wide-angle X-ray diffraction (XRD) pattern of the Au/OMS composites display typical wide diffraction peaks assigned to the fcc structure of Au nanoparticles (Figure S8a). The mean crystalline size is calculated from the Debye−Scherrer formula to be about 3.2 nm. Such a small size is attributed to the confined aggregation of the Au nanoparticles on the surface of the ultralarge mesopore. The UV−vis absorption spectrum of the Au/OMS composite dispersed in an aqueous solution shows an extinction peak centered at ~551 nm, which is due to the surface plasmonic resonance of nanosized Au nanoparticles supported on silica (Figure S8b). TEM images and corresponding fast Fourier transforms show that the Au/OMS composite has a high degree of periodicity viewed from [110] and [211] directions, respectively (Figure 6a,b). It suggests that the ordered mesostructure of the silica support is well retained after loading Au nanoparticles. Selected area electron diffraction (SAED) pattern shows spotty diffraction rings assigned to the fcc structured Au crystalline nanoparticles (Figure 6b, insert). High-magnification TEM images (Figure 6c) reveal that uniform Au nanoparticles (~4.0 nm) are homogeneously confined in the surface of the silica mesopores. HR-TEM images of Au nanoparticles clearly show the lattice fringes with a spacing of about 0.23 nm, which corresponds to the spacing of the (111) planes of single crystalline Au (Figure 6d). Nitrogen adsorption−desorption measurement indicates that the Au/OMS sample has a BET surface area of 309 m^2/g and pore volume of 1.10 cm^3/g, both slightly lower than those of parent mesoporous silica due to the incorporation of gold nanoparticles.

The reduction of 4-nitrophenol (4-NP) by sodium borohydride ($NaBH_4$) was chosen as a model reaction to investigate the catalytic activity of the Au/OMS composite. The 4-NP solution exhibits a strong absorption peak at 317 nm. The absorption peak shifts to 400 nm upon addition of excess amount of $NaBH_4$ solution due to the formation of 4-nitrophenolate ions.[60−62]

After the addition of the Au/OMS catalyst, the absorption peak at ~400 nm significantly decreases with the time. A new peak appears at around 305 nm, indicating the reduction of 4-NP to 4-aminophenol (4-AP) (Figure 7a). Considering the reductant concentration is much higher than that of 4-NP ($C_{NaBH4}/C_{4\text{-NP}}$ = 876), the reduction should be of first order with regard to the reactant.[60] Because the absorbance is proportional to the concentration of 4-NP in this system, the value of $\ln(A_t/A_0)$ reflects the change of $\ln(C_t/C_0)$. The kinetic constant k is calculated to be 0.0583 min^{-1} from the curve of $\ln(C_t/C_o)$ versus reaction time (Figure 7b). Because of the large particle size of the mesoporous silica, the Au/OMS composite can be easily recycled and washed after the reaction by centrifugation. The results show that the recycled catalyst has similar catalytic performance even after running for 10 times, reflecting a good reusability. The excellent catalytic performance should be attributed to the highly dispersed and confined small Au nanoparticles, as well as the 3-D large-pore ordered mesoporous silica with large accessible entrances which provide high surface area and efficient mass transport (Figure 7a, insert).

4. CONCLUSIONS

In summary, a solvent evaporation induced aggregating assembly (EIAA) approach has been demonstrated for the synthesis of highly ordered mesoporous silica materials with large mesopores and window sizes by using water-insoluble block copolymer with large molecular weight as a template in a blend solvent containing a good solvent and a poor solvent (water). The mesoporous silica materials prepared by using PEO-*b*-PMMA as a template and TEOS as a precursor in the acidic THF/H_2O mixture medium have ordered fcc mesostructure, large tunable pore size of up to 37.0 nm, large window size (8.7 nm), high surface area (508 m^2/g), and large pore volume (1.46 cm^3/g). Interestingly, the mesoporous silicas obtained from the EIAA approach show crystal-like morphology with large particle size (0.5−6 μm). A mechanism which involves a good solvent evaporation induced continuous formation and aggregating and packing of the spherical silica/copolymer micelles on the interface of water-rich phase is proposed. The Au/OMS composites with well-dispersed Au nanoparticles (~4 nm) showed an excellent catalysis for fast and efficient reduction of 4-nitrophenol at room temperature. Because of highly confined small Au nanoparticles, the Au/OMS catalysts can be reusable without significant decrease of catalysis performance even after 10 cycles. Moreover, it is believed that this unique EIAA process provides a novel approach and can be extended to synthesize various large-pore ordered mesoporous materials by choosing abundant large copolymers such as PEO-*b*-PS, PEO-*b*-PI as a template and using diverse precursors, such as metal salts, metal alkoxides, and/or various colloidal nanoparticles.

■ ASSOCIATED CONTENT

Supporting Information. TEM images of the PEO-*b*-PMMA block polymers obtained through EIAA without TEOS. SAXS patterns, TEM images, N_2 sorption isotherms, and pore size distributions of ordered mesoporous silica using EO_{44}-*b*-MMA_{103} as the template. Cryo-SEM images of the samples withdrawn from the reaction solution of EO_{124}-*b*-MMA_{174}/TEOS/2 M HCl/THF/H_2O as function of the evaporation time and corresponding hollow silica spheres after calcination. DLS spectra and wide-angle XRD pattern UV−vis spectrum of the gold-nanoparticle incorporated mesoporous silica (Au/OMS) composites dispersed in water solution. This material is available free of charge via the Internet at http://pubs.acs.org.

■ AUTHOR INFORMATION

Corresponding Author
dyzhao@fudan.edu.cn; yhdeng@fudan.edu.cn

■ ACKNOWLEDGMENT

This work was supported by NSF of China (20890123, 20821140537, 21073040 and 20871030), State Key 863 Program of PRC (2009AA033701), Shanghai Leading Academic Discipline Project (B108), and Science & Technology Commission of Shanghai Municipality (08DZ2270500) and Fudan Graduate Innovation Funds.

■ REFERENCES

(1) Hartmann, M. *Chem. Mater.* **2005**, *17*, 4577.
(2) Fan, J.; Yu, C. Z.; Gao, T.; Lei, J.; Tian, B. Z.; Wang, L. M.; Luo, Q.; Tu, B.; Zhou, W. Z.; Zhao, D. Y. *Angew. Chem., Int. Ed.* **2003**, *42*, 3146.
(3) Deng, Y. H.; Qi, D. W.; Deng, C. H.; Zhang, X. M.; Zhao, D. Y. *J. Am. Chem. Soc.* **2008**, *130*, 28.
(4) Grün, M.; Kurganov, A. A.; Schacht, S.; Schüth, F.; Unger, K. K. *J. Chromatogr., A* **1996**, *740*, 1–9.
(5) Gallis, K. W.; Araujo., J. T.; Duff, K. J.; Moore, J. G.; Landry, C. C. *Adv. Mater.* **1999**, *11*, 1452.
(6) Zhao, J. W.; Gao, F.; Fu, Y. L.; Jin, W.; Yang, P. Y.; Zhao, D. Y. *Chem. Commun.* **2002**, 752.
(7) Stein, A. *Adv. Mater.* **2003**, *15*, 763.
(8) Corma., A. *Chem. Rev.* **1997**, *97*, 2373.
(9) Taguchi, A.; Schüth, F. *Microporous Mesoporous Mater.* **2005**, *77*, 1.
(10) Wan, Y.; Shi, Y. F.; Zhao, D. Y. *Chem. Commun.* **2007**, 897.
(11) Wan, Y.; Zhao, D. Y. *Chem. Rev.* **2007**, *107*, 2821.
(12) Deng, Y. H.; Cai, Y.; Sun, Z. K.; Liu, J.; Liu, C.; Wei, J.; Li, W.; Liu, C.; Wang, Y.; Zhao, D. Y. *J. Am. Chem. Soc.* **2010**, *132*, 8466.
(13) Ma, G. C.; Yan, X. Q.; Li, Y. L.; Xiao, L. P.; Huang, Z. J.; Lu, Y. P.; Fan, J. *J. Am. Chem. Soc.* **2010**, *132*, 9596.
(14) Lai, C. Y.; Trewyn, B. G.; Jeftinija, D. M.; Jeftinija, K.; Xu, S.; Jeftinija, S.; Lin, V. S.-Y. *J. Am. Chem. Soc.* **2003**, *125*, 4451.
(15) Giri, S.; Trewyn, B. G.; Stellmaker, M. P; Lin, V. S.-Y. *Angew. Chem., Int. Ed.* **2005**, *117*, 5166.
(16) Torney, F.; Trewyn, B. G.; Lin, V. S.-Y.; Wang, K. *Nat. Nanotechnol.* **2007**, *2*, 295.
(17) Vivero-Escoto, J. L.; Slowing, I. I.; Wu, C.-W.; Lin, V. S.-Y. *J. Am. Chem. Soc.* **2009**, *131*, 3462.
(18) Liu, R.; Zhang, Y.; Zhao, X.; Agarwal, A.; Mueller, L. J.; Feng, P. Y. *J. Am. Chem. Soc.* **2010**, *132*, 1500.
(19) Mamak, M.; Coomb, N.; Ozin, G. *J. Am. Chem. Soc.* **2000**, *122*, 8932.
(20) Joo, S. H.; Choi, S. J.; Oh, I.; Kwak, J.; Liu, Z.; Terasaki, O.; Ryoo, R. *Nature* **2001**, *412*, 169.
(21) Pereira, F.; Valle, K.; Belleville, P.; Morin, A.; Lambert, S.; Sanchez, C. *Chem. Mater.* **2008**, *20*, 1710.
(22) Kresge, C. T.; Leonowicz, M. E.; Roth, W. J.; Vartuli, J. C.; Beck, J. S. *Nature* **1992**, *359*, 710.
(23) Zhao, D. Y.; Feng, J. L.; Huo, Q. S.; Melosh, N.; Fredrickson, G. H.; Chmelka, B. F.; Stucky, G. D. *Science* **1998**, *279*, 548.
(24) Che, S.; Liu, Z.; Ohsuna, T.; Sakamoto, K.; Terasaki, O.; Tatsumi, T. *Nature* **2004**, *429*, 281.
(25) Yang, P. D.; Zhao, D. Y.; Margolese, D. I.; Chmelka, B. F.; Stucky, G. D. *Nature* **1998**, *396*, 152.

(26) Meng, Y.; Gu, D.; Zhang, F. Q.; Shi, Y. F.; Yang, H. F.; Li, Z.; Yu, C. Z.; Tu, B.; Zhao, D. Y. *Angew. Chem., Int. Ed.* **2005**, *44*, 7053.
(27) Zhang, F. Q.; Meng, Y.; Gu, D.; Yan, Y.; Yu, C. Z.; Tu, B.; Zhao, D. Y. *J. Am. Chem. Soc.* **2005**, *127*, 13508.
(28) Liang, C. D.; Dai, S. *J. Am. Chem. Soc.* **2006**, *128*, 5316.
(29) Lin, H. P.; Mou, C. Y. *Acc. Chem. Res.* **2002**, *35*, 927.
(30) Yamauchi, Y.; Kuroda, K. *Chem.—Asian J.* **2008**, *3*, 664.
(31) Kimura, T.; Kuroda, K. *Adv. Funct. Mater.* **2009**, *19*, 511.
(32) Templin, M.; Franck, A.; DuChesne, A.; Leist, H.; Zhang, Y. M.; Ulrich, R.; Schadler, V.; Wiesner, U. *Science* **1997**, *278*, 1795.
(33) Deng, Y. H.; Yu, T.; Wan, Y.; Shi, Y. F.; Meng, Y.; Gu, D.; Zhang, L. J.; Huang, Y.; Liu, C.; Wu, X. J.; Zhao, D. Y. *J. Am. Chem. Soc.* **2007**, *129*, 1690.
(34) Lu, Y. F.; Ganguli, R.; Drewien, C. A.; Anderson, M. T.; Brinker, C. J.; Gong, W. L.; Guo, Y. X.; Soyez, H.; Dunn, B.; Huang, M. H.; Zink, J. I. *Nature* **1997**, *389*, 364.
(35) Brinker, C. J.; Lu, Y. F.; Sellinger, A.; Fan, H. Y. *Adv. Mater.* **1999**, *11*, 579.
(36) Grosso, D. *Adv. Funct. Mater.* **2004**, *14*, 309.
(37) Nicole, L.; Boissière, C.; Grosso, D.; Quach, A.; Sanchez, C. *J. Mater. Chem.* **2005**, *15*, 3598.
(38) Hudson, S.; Cooney, J.; Magner, E. *Angew. Chem., Int. Ed.* **2008**, *47*, 8582.
(39) Fan, J.; Shui, W. Q.; Yang, P. Y.; Wang, X. Y.; Xu, Y. M.; Wang, H. H.; Chen, X.; Zhao, D. Y. *Chem.—Eur. J.* **2005**, *11*, 5391.
(40) Deng, Y. H.; Cai, Y.; Sun, Z. K.; Gu, D.; Wei, J.; Li, W.; Guo, X. H.; Yang, J. P.; Zhao, D. Y. *Adv. Funct. Mater.* **2010**, *20*, 3658.
(41) Sun, Z. K.; Deng, Y. H.; Wei, J.; Gu, D.; Tu, B.; Zhao, D. Y. *Chem. Mater.* **2011**, *23*, 2176.
(42) Deng, Y. H.; Liu, J.; Liu, C.; Gu, D.; Sun, Z. K.; Wei, J.; Zhang, J. Y.; Zhang, L. J.; Tu, B.; Zhao, D. Y. *Chem. Mater.* **2008**, *20*, 7281.
(43) Yu, K.; Hurd, A. J.; Eisenberg, A; Brinker, C. J. *Langmuir* **2001**, *17*, 7692.
(44) Smarsly, B.; Xomeritakis, G.; Yu, K.; Liu, N. G.; Fan, H. Y.; Assink, R. A.; Drewien, C. A.; Ruland, W.; Brinker, C. J. *Langmuir* **2003**, *19*, 7295.
(45) Yu, K.; Smarsly, B.; Brinker, C. J. *Adv. Funct. Mater.* **2003**, *13*, 47.
(46) Lee, J.; Orilall, M. C.; Warren, S. C.; Kamperman, M.; Disalvo, F. J.; Wiesner, U. *Nat. Mater.* **2008**, *7*, 222.
(47) Grosso, D.; Boissiere, C.; Smarsly, B.; Brezesinski, T.; Pinna, N.; Albouy, P. A.; Amenitsch, H.; Antonietti, M.; Sanchez, C. *Nat. Mater.* **2004**, *3*, 787.
(48) Kuang, D. B.; Brezesinki, T.; Smarsly, B. *J. Am. Chem. Soc.* **2004**, *126*, 10534.
(49) Deng, Y. D; Liu, C.; Gu, D.; Yu, T.; Tu, B.; Zhao, D. Y. *J. Mater. Chem.* **2008**, *18*, 91.
(50) Wei, J.; Deng, Y. H.; Zhang, J. Y.; Sun, Z. K.; Tu, B.; Zhao, D. Y. *Solid State Sci.* **2011**, *13*, 784.
(51) Zhang, J. Y.; Deng, Y. H.; Gu, D.; Wang, S. T.; She, L.; Che, R. C.; Wang, Z. S.; Tu, B.; Xie, S. H.; Zhao, D. Y. *Adv. Energy Mater.* **2011**, *1*, 241.
(52) Chen, M. Q.; Kishida, A.; Serizawa, T.; Akashi, M. *J. Polym. Sci., Part A: Polym. Chem.* **2000**, *38*, 1811.
(53) Yabu, H.; Higuchi, T.; Shimomura, M. *Adv. Mater.* **2005**, *17*, 2062.
(54) Hussain, H.; Tan, B. H.; Seah, G. L.; Liu, Y.; He, C. B.; Davis, T. P. *Langmuir* **2010**, *26*, 11763.
(55) Wyman, I.; Njikang, G.; Liu, G. J. *Prog. Polym. Sci.* **2011**, *36*, 1152.
(56) Zhu, H. G.; Liang, C. D.; Yan, W. F.; Overbury, S. H.; Dai, S. *J. Phys. Chem. B* **2006**, *110*, 10842.
(57) Fan, J.; Yu, C. Z.; Lei, J.; Zhang, Q.; Li, T. C.; Tu, B.; Zhou, W. Z.; Zhao, D. Y. *J. Am. Chem. Soc.* **2005**, *127*, 10794.
(58) Broekhoff, J. C. P.; deBoer, J. H. *J. Catal.* **1967**, *9*, 8.
(59) Woodcock, L. V. *Nature* **1997**, *385*, 141.
(60) Pradhan, N.; Pal, A.; Pal, T. *Langmuir* **2001**, *17*, 1800.
(61) Pradhan, N.; Pal, A.; Pal, T. *Colloids Surf., A* **2002**, *196*, 247.
(62) Ghosh, S. K.; Mandal, M.; Kundu, S.; Nath, S.; Pal, T. *Appl. Catal., A* **2004**, *268*, 61.